2023

Schizo-Net: A novel Schizophrenia Diagnosis Framework Using Late Fusion Multimodal Deep Learning on Electroencephalogram-Based Brain Connectivity Indices

Nitin Grover
Thapar Institute of Engineering and Technology Patiala, Punjab, India

Aviral Chharia
Thapar Institute of Engineering and Technology Patiala, Punjab, India

Rahul Upadhyay
Thapar Institute of Engineering and Technology Patiala, Punjab, India

See next page for additional authors

Funder: Artificial Intelligence and Cognitive Load Research Laboratory, Technological University Dublin

Schizo-Net: A *novel* Schizophrenia Diagnosis Framework Using Late Fusion Multimodal Deep Learning on Electroencephalogram-Based Brain Connectivity Indices

Nitin Grover, Aviral Chharia, *Member, IEEE*, Rahul Upadhyay, and Luca Longo

***Abstract*— Schizophrenia (SCZ) is a serious mental condition that causes hallucinations, delusions, and disordered thinking. Traditionally, SCZ diagnosis involves the subject's interview by a skilled psychiatrist. The process needs time and is bound to human errors and bias. Recently, brain connectivity indices have been used in a few pattern recognition methods to discriminate neuropsychiatric patients from healthy subjects. The study presents *Schizo-Net*, a novel, highly accurate, and reliable SCZ diagnosis model based on a late multimodal fusion of estimated brain connectivity indices from EEG activity. First, the raw EEG activity is pre-processed exhaustively to remove unwanted artifacts. Next, six brain connectivity indices are estimated from the windowed EEG activity, and six different deep learning architectures (with varying neurons and hidden layers) are trained. The present study is the *first* which considers a large number of brain connectivity indices, especially for SCZ. A detailed study was also performed that identifies SCZ-related changes occurring in brain connectivity, and the vital significance of BCI is drawn in this regard to identify the biomarkers of the disease. *Schizo-Net* surpasses current models and achieves 99.84% accuracy. An optimum deep learning architecture selection is also performed for improved classification. The study also establishes that Late fusion technique outperforms single architecture-based prediction in diagnosing SCZ.**

***Index Terms*— Schizophrenia, deep learning, brain connectivity features, feature fusion, classification.**

Manuscript received 28 March 2022; revised 22 July 2022, 23 September 2022, and 4 December 2022; accepted 9 January 2023. Date of publication 20 January 2023; date of current version 2 February 2023. This work was supported in part by the Artificial Intelligence and Cognitive Load Research Laboratory, Applied Intelligence Research Centre, Technological University Dublin, Ireland; and in part by the Thapar Institute of Engineering and Technology Seed Money Grant for the Project "Analysis of Electroencephalogram Signals for implementation of P300-based Brain Computer Interface". *(Corresponding author: Luca Longo.)*

Nitin Grover and Rahul Upadhyay are with the Department of Electronics and Communication Engineering, Thapar Institute of Engineering and Technology, Patiala, Punjab 147004, India.

Aviral Chharia is with the Department of Mechanical Engineering, Thapar Institute of Engineering and Technology, Patiala, Punjab 147004, India.

Luca Longo is with the Artificial Intelligence and Cognitive Load Research Laboratory, Applied Intelligence Research Centre, School of Computer Science, Technological University Dublin, Dublin 7, D07 EWV4 Ireland (e-mail: luca.longo@tudublin.ie).

This article has supplementary downloadable material available at https://doi.org/10.1109/TNSRE.2023.3237375, provided by the authors.

Digital Object Identifier 10.1109/TNSRE.2023.3237375

I. Introduction

SCHIZOPHRENIA (SCZ) is a serious mental disorder that impacts an individual's ability to think, feel and behave clearly. Moreover, continuous recurrent episodes of psychosis are a common disorder condition [1]. Hallucinations (seeing things or hearing voices that aren't there), delusions (fixed, incorrect beliefs), paranoia, and disorganized thinking are other frequently complained occurrences [2]. In recent years, SCZ has been considered a disorder of "dysconnectivity". Dysconnectivity of the pre-frontal cortex is caused by developing hippocampal injuries, according to animal models [3]. Soon the concept of SCZ was derived considering that both heredity and organic brain ailment were implicated [4]. However, until Johnstone et al. published research employing computed tomography in 1976, the organic aspects of the disease were overlooked. The condition usually appears in early adulthood, but it is reported that men have a peak incidence about a decade earlier than women [5]. The reason behind this is still unclear. An equally puzzling but consistent finding is the slight excess of births of people with SCZ in the cold winter [6]. Thus environmental factors too seem to be associated with winter birth that causes neural damage in the fetus/neonate. The cause could be a viral infection, seasonal difference, or other complications during pregnancy or delivery [7], [8]. Nevertheless, a well-defined methodology to treat SCZ is lacking.

A. Background

SCZ related abnormalities are very small and subtle, and thus this makes the detection of the disorder to be complicated without advanced technology. MRI imaging has shown the presence of structural brain abnormalities in SCZ patients. There is also evidence that the abnormalities are neuro-developmental in origin but unfold later in development [9]. However, these abnormalities usually become evident only when the patient develops symptoms. Moreover, as many different brain regions are involved in the neuropathology of SCZ, disturbance in the functioning of a particular brain region cannot fully explain the range of various impairments. Therefore, new models need to be developed and tested to explain neural circuitry abnormalities affecting brain regions, "not necessarily structurally proximal" to each

other but functionally interrelated [10]. According to WHO, SCZ can be treated [11]; however, its treatment involves long-term medication and requires early detection of the disease. Determining nervous system damage is tricky since most symptoms overlap in combinations among the different disorders. Similar disorders do not have definitive sources, unique markers, or tests, making diagnosing a neurological disease laborious. Usually, complete medical history and physical exam are used to diagnose such disorders. Moreover, highly trained and experienced experts are needed for correct diagnosis. Other tests might be used, including computed tomography (CT), Magnetic Resonance Imaging (MRI), Ultrasound, and Electroencephalogram. Electroencephalogram (EEG) is a non-invasive technique that records the brain's electrical activity through scalp-connected electrodes. It has been found to help detect a range of neural disorders, viz., brain tumors, inflammations, sleep disorders, and stroke. Due to its portability, non-invasiveness, and excellent temporal resolution, EEG has gained a reputation as a preferred brain imaging tool for diagnosing neurological diseases with high accuracy [12], [13], [14].

B. Motivation

In recent years, deep learning methods have been developed to detect various neurological disorders that utilize EEG signals [15], [75] and solve various classification tasks [76], [77], [78]. Although these methods work well in finding hidden features and patterns from the non-linear data, they struggle to attain higher-classification accuracy on EEG due to the data being highly complex and the frequent non-cerebral contamination that accompanies it [61], [62]. Cortically generated EEG is often contaminated by non-cerebral artifact origins such as eye blinks, ocular movements, Electrocardiogram (ECG), and Electromyogram (EMG) artifacts. Therefore, it becomes imperative to clean recorded EEG activity before extracting information and training deep learning models [16], [17]. Various methods for the SCZ detection using EEG have been explored. Siuly et al. [18] suggested a method using Empirical Mode Decomposition to handle non-stationary, nonlinear EEG signals, decomposed them into intrinsic mode functions and calculated 21 statistical features. Among the considered classifiers, the ensemble bagged tree classifier produced the best classification accuracy of 93.21%. In another work, Khare et al. [19] used a combination of time-frequency graphs and CNNs to classify SCZ patients and reported an accuracy of 93.36% using the smoothed pseudo-Wigner–Ville distribution-based time-frequency representation. Oh et al. [20] collected EEG data from 14 healthy subjects and 14 SCZ patients and proposed an 11-layered CNN architecture for the classification. The proposed model generated a classification accuracy of 98.07% and 81.26% for non-subject-based and subject-based testing, respectively. In another work, Jahmunah et al. [21] proposed an automated diagnostic tool to detect SCZ, extracting 157 features from both classes. An optimal feature set of 14 was selected using a t-test [22] and an accuracy of 92.91% was achieved for SVM. Dvey-Aharon et al. [23] designed a SCZ detection and classification methodology by advanced analysis of EEG recordings using a single electrode, reporting an accuracy of 88.7%. Recently, brain connectivity measures (as features) have been deemed suitable for classifying EEG activity. The brain is a large network of neurons, and synchronous neural activities at different regions can provide useful information, referred to as brain connectivity. Connectivity between brain regions can be anatomical (structural), functional (by functional integration of separated regions) and casual relationship (effective) [24]. The relationship between brain regions can be described as a brain network whose vertices and edges correspond to brain regions and their connections. If the edges are weighted, they represent the strength of connections with continuous values. Then, an adjacency matrix can be defined, whose elements are the strength of connections between two electrodes [25]. Moon et al. [26] proposed a CNN-based system to learn the representation of neural activities based on brain connectivity to classify emotions in a video by using three different connectivity measures, including Pearson Correlation Coefficient (PCC), Phase Locking Value (PLV), and Transfer Entropy (TE). The highest accuracy of 87.36% is obtained using the PLV measure with a kernel size of 5. Phang et al. [27] proposed a DNN with deep belief network for automated SCZ classification. This study suggested the usage of vector auto-regression-based Directed Connectivity (DC), graph-theoretical Complex Network (CN), and its combination as input features. It is reported that the Combined DC-CN features provide better classification performance with the highest classification accuracy of 95%.

C. Contributions

The present work aims to present *Schizo-Net*, a framework for reliable and high accuracy SCZ detection using late fusion multimodal deep learning on EEG-based brain connectivity measures. Here, we extract information about the disrupted brain connectivity in an SCZ brain, various phenomena such as synchronization between different brain regions, the directionality of the information, and the correlation of signals have been analyzed. Six connectivity measures have been estimated [28], [29], [30], [31], [32], [33]. The estimated measure helps quantify synchronization and provides information on directionality and causality. The output of these methods was analyzed and exported in matrices. These feature matrices are then used as input to the neural networks. In the present work, we tested several neural network architectures with varying numbers of neurons and hidden layers. It is observed from the experimentation that neural networks were able to learn latent details of the EEG connectivity patterns. Further, late fusion method is implemented and examined to combine the results of different neural networks trained on different connectivity methods. The contributions of the present study include-

1) The present study is the *first* to provide a comparative study taking into consideration a large number of brain connectivity indices for SCZ using EEG.
2) We perform late multimodal feature fusion to evaluate the efficacy of combined feature vectors for SCZ diagnosis. For classification, five different DNN architectures are implemented and evaluated. (Section II, III)

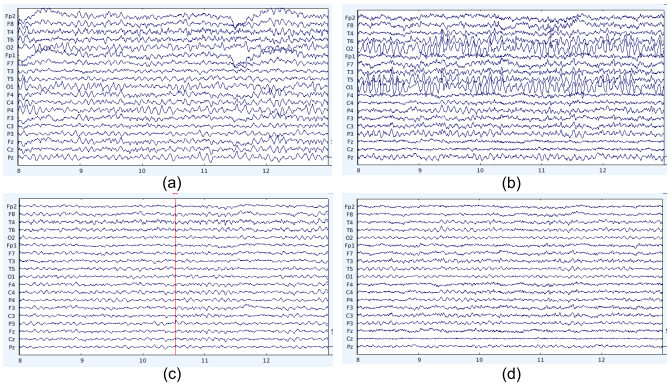

Fig. 1. Raw EEG signal associated with an (a) SCZ patient and an (b) Healthy patient. EEG signal after undergoing Makoto's preprocessing for the (c) SCZ patient and (d) Healthy patient.

3) Compared to the previous studies, Schizo-Net achieves state-of-the-art results for the fused feature vectors.
4) We also demonstrate experimentally that late fusion outperforms single architecture-based prediction. (Table II)
5) Compared to previous studies, a detailed study has also been performed that identifies SCZ-related changes that occur in brain connectivity, and the vital significance of brain connectivity indices is drawn in this regard to identify the biomarkers of the disease. (Section III)

II. Materials and Methods

A. Participants and EEG Recording

The EEG data from 14 patients (7 males: 27.9 ± 3.3 years, 7 females: 28.7 ± 4.1 years) was recorded by the Institute of Psychiatry and Neurology in Warsaw, Poland [34]. The data for fourteen healthy subjects (7 males: 26.8 ± 2.9 years, 7 females: 28.7 ± 3.4 years) were also recorded by the same institute. Fifteen minutes of data was acquired at 250Hz sampling frequency in a composed state with eyes closed on standard 19 channel (which includes Fp1, Fp2, F7, F3, Fz, F4, F8, T3, C3, Cz, C4, T4, T5, P3, Pz, P4, T6, O1 and O2) based 10-20 EEG montage. Fig. 1 depicts the sample EEG signals where healthy individuals show enhanced amplitude values in most channels compared to those of SCZ patients.

B. Pre-Processing

During recording, ongoing EEG activity is frequently contaminated by non-cerebral artifacts originating from ocular movements, Electrocardiogram (ECG), and Electromyogram (EMG) artifacts. Moreover, other sources, including background electrical disturbances, noise due to instrumentation, and external electromagnetic activity, also affect the recording. This strong presence of artifacts diminishes the EEG signal quality and may cause erroneous classification. Therefore, it is essential to eliminate artifacts and noise before feature estimation [35]. Preprocessing aims to remove artifacts, improve stationarity, and increase the SNR of the recorded EEG activity. To clean contaminated EEG activity, Makoto's preprocessing pipeline is implemented using the EEGLAB toolbox [36] in MATLAB software. Initially, offset correction is performed on the recorded EEG activity. Next, the channel location data is added, which is essential to understand which channel montage is being followed. Since the continuous EEG data needs to be filtered before epoching or artifact removal, a basic Finite Impulse Response filter is used. Filtering before epoching minimizes the introduction of filtering artifacts at epoch boundaries. The main focus is on the alpha band frequency signal, so the lower and higher edges of the frequency pass band are set accordingly [37]. The EEGLAB algorithm automatically estimates the filter order for the FIR filter.

After filtering, the artifacts are automatically rejected, starting from detecting any bad channels in the data. That is, the channels that are either noisy all the time or are completely flat are removed from the dataset. Next, the rejection of bad portions of data is done using Artifact Subspace Reconstruction (ASR) algorithm [38]. ASR first finds the clean portion of the data, which is referred to as the "calibration data." If a particular data region exceeds 20 times the standard deviation of this calibration data, ASR rejects it. Independent Component Analysis (ICA) is the final pre-processing step [39]. It subtracts embedded artifacts from muscle and eye movements and identifies brain sources from which a particular signal originates. We use Information maximization (Infomax) ICA in this study. Compared to *FastICA*, *Infomax ICA* rapidly converges and separates the estimated sources more efficiently. It has better results, but it is more mathematically complex than FastICA, thus requiring more computational resources [40]. For identifying decomposed ICs as artifactual/ non-artifactual, the "ADJUST" processing pipeline is followed [72]. The identified artifactual ICs were subtracted, and inverse ICA was performed to regenerate artifact-free EEG activity.

Architecture 1			
Layer	**Type**	**Number of neurons**	**Activation**
1	Input (Flatten)	-	-
2	Dense	2	ReLU
3	Output	2	Softmax

Architecture 2			
Layer	**Type**	**Number of neurons**	**Activation**
1	Input (Flatten)	-	-
2	Dense	4	ReLU
3	Output	2	Softmax

Architecture 3			
Layer	**Type**	**Number of neurons**	**Activation**
1	Input (Flatten)	-	-
2	Dense	16	ReLU
3	Output	2	Softmax

Architecture 4			
Layer	**Type**	**Number of neurons**	**Activation**
1	Input (Flatten)	-	-
2	Dense	32	ReLU
3	Output	2	Softmax

Architecture 5			
Layer	**Type**	**Number of neurons**	**Activation**
1	Input (Flatten)	-	-
2	Dense	16	ReLU
3	Dense	32	ReLU
4	Output	2	Softmax

Fig. 2. Layer-wise overview of NNET architectures 1-5.

C. Feature Extraction

In this study, multiple connectivity features are used to capture the neural synchronous activity in different brain

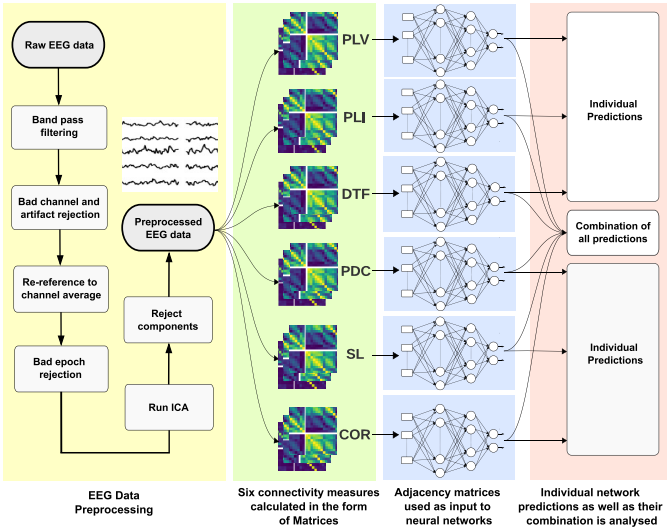

Fig. 3. Illustration of *Schizo-Net* and its flow for EEG pre-processing, feature extraction and late fusion classification.

regions. This is mainly done to get an overall picture of brain connectivity. There are 3 connectivities- *structural*, *functional* and *effective*. Structural connectivity refers to the connectivity between brain regions which are anatomically connected, while functional connectivity is based on the functional integration of different brain regions. In contrast, effective connectivity is based on a causal relationship [24]. In graph theory, the brain is modeled as a network consisting of nodes representing the brain's different areas or the EEG channels, with edges between them representing the connectivity between those respective nodes [34]. In the present study, six brain connectivity measures are used to compute these matrices, namely Phase-Locking Value (PLV), Partial Directed Coherence (PDC), Phase-Lag Index (PLI), Synchronization Likelihood (SL), Directed Transfer Function (DTF), Pearson's Correlation Coefficient (COR). Here, PLV and PLI provide information about phase synchronization, whereas DTF and PDC allow quantifying the causal interactions between brain regions and provide directions of information flow. SL estimates the generalized synchronization, whereas COR provides information on linear correlations within data. Each preprocessed EEG data segment has a length of 6.5 minutes. Further, the HERMES toolbox [41] is used to perform windowing on the cleaned EEG activity segment with the window length of 1 minute, overlapping 80% between windowed segments. Windowing helps in obtaining a temporal resolution to calculated indices with more trials. The segmentation led to 25 EEG trials corresponding to each subject. From the HERMES toolbox, the extracted data for each index was in the shape of (1, 28). Each element was a 4D matrix (Channels × Channels × Frequency Band × Windows). It is important to express a set of connection features as a 2D matrix to use them as an input to neural networks. This data was then transformed into the shape of (784, 2), where the first element of each row contains a (19 × 19) matrix and the second element is the label in one hot encoded format ([1,0] for H; [0,1] for Sz). Thus, we transformed all connectivity features into a 19 × 19 connectivity matrix, whose (i^{th}, j^{th}) elements represent connectivity between the i^{th} and j^{th} electrodes.

D. Brain Connectivity Measures

1) Phase Locking Value (PLV): Phase locking value (PLV) is a functional connectivity metric that relies on the instantaneous time-series phase [28]. It assumes that when two brain regions are functionally connected, the difference between their immediate phases of signals should be constant. PLV uses relative phase difference only and is defined as:

$$PLV = |e^{i\,\Delta\phi_{rel}(t)}| = \left|\frac{1}{N}\sum_{n=1}^{N} e^{i\,\Delta\phi_{rel}(t)}\right| = \sqrt{\cos\Delta\phi_{rel}(t)^2 + \sin\Delta\phi_{rel}(t)^2} \quad (1)$$

where $\Delta\phi_{rel}(t)$ represents the relative phase difference at an arbitrary time t. The phase difference can vary between 0 and 1, representing completely independent or perfectly synchronized signals. PLV estimates the relative phase distribution over the unit circle. When X and Y are strongly phase synchronized, the relative phase occupies a portion of the circle, and the PLV is close to 1. If the signals are not synchronized, the relative phase spreads across the unit circle, and the PLV remains low. When dealing with continuous data rather than evoked responses, PLV is also referred to as "Mean Phase Coherence" [42]. Nevertheless, PLV has certain limitations. It is prone to volume conduction effects. The volume conduction effect is the transmission of electric current through the human tissue towards the sensors, and therefore a single source may be seen by multiple electrodes, which can result in spurious PLV values [43].

2) Phase Lag Index (PLI): Phase Lag Index (PLI) addresses PLV's limitations, explicitly eliminating the volume conduction effect [43]. It measures the asymmetry of phase difference distributions between two signals [29]. PLI is defined as,

$$PLI = |\text{sign}(\Delta\phi_{rel}(t))| = \left|\frac{1}{N}\sum_{n=1}^{N}\text{sign}(\Delta\phi_{rel}(t_n))\right| \quad (2)$$

where $\Delta\phi_{rel}(t)$ represents the relative phase difference at an arbitrary time t. However, PLI discards a significant component of genuine interactions in doing so. It discards phase distributions centered around 0 and π to be robust against the presence of common sources. Thus, mitigating the volume conduction effect [41]. However, discontinuity in this measure limits its sensitivity to noise and volume conduction since tiny perturbations change phase lags into leads and vice versa. For small-magnitude synchronization effects, this problem might become problematic.

3) Directed Transfer Function (DTF): Directed Transfer Function (DTF) measures the information flow between multivariate spectral components [31]. The DTF is defined in the frequency domain being based on Granger Causality and models the time series by Multivariate Auto-regressive (MVAR) processes. In the MVAR model, only lagged effects are modeled among the time series, while instantaneous effects are forsaken [44]. An MVAR process of order p and dimension M, i.e., $x_1(t), \ldots, x_M(t)$ is given by:

$$\begin{pmatrix} x_1(t) \\ \vdots \\ x_M(t) \end{pmatrix} = \sum_{r=1}^{p} Ar \begin{pmatrix} x_1(t-r) \\ \vdots \\ x_M(t-r) \end{pmatrix} + \begin{pmatrix} \epsilon_1(t) \\ \vdots \\ \epsilon_M(t) \end{pmatrix} \quad (3)$$

where Ar is a $M \times M$ coefficients matrix, and $\epsilon_1(t), \epsilon_2(t), \ldots, \epsilon_M(t)$ are independent Gaussian white noises with covariance matrix $\sum$. Let $X(t) = \begin{pmatrix} x_1(t) \\ \vdots \\ x_M(t) \end{pmatrix}$ and $E(t) = \begin{pmatrix} \epsilon_1(t) \\ \vdots \\ \epsilon_M(t) \end{pmatrix}$. On transforming to frequency domain,

$$E(f) = A(f).X(f) \tag{4}$$

$$X(f) = A^{-1}(f).E(f) = H(f).E(f) \tag{5}$$

where $H(f)$ is the system transfer matrix representing the relationships between signals and their spectral characteristics. Here, DTF is defined by:

$$DTF^2(f) = \frac{|H_{ij}(f)|^2}{\sum_{n=1}^{k} |H_{in}(f)|^2} \tag{6}$$

where $H_{ij}(f)$ is an element of a transfer matrix $H(f)$ of the MVAR model. DTF represents the causal influence of channel j^{th} on channel i^{th} at frequency f. This connectivity measure determines the directional impacts between any given pair of channels in a multivariate data set.

4) Partial Directed Coherence (PDC): Partial Directed Coherence (or PDC) provides a frequency-domain measure based on Granger causality [32]. DC tells us whether and how two structures under consideration are functionally connected. DC emphasizes their relative structural links by breaking their interactions into "feed-forward" and "feedback" components, whereas ordinary coherence focuses on the structures themselves and the reciprocal synchronicity of their activity. PDC was developed as a result, and it leads to structural information while simultaneously modeling several time series. It is based on modeling time series by multivariate autoregressive (MVAR) and is used to reveal the direction of information flow between different brain areas. Mathematically:

$$P_{uv}(f) = \frac{A_{uv}(f)}{\sqrt{a_v^*(f) a_v(f)}} \tag{7}$$

where $A_{uv}(f)$ is an element of $A(f)$, which is a Fourier transform of the MVAR model coefficients $A(t)$, $a_v(f)$ is the v^{th} column of $A(f)$, and the asterisk mark represents the transpose and complex conjugate operations. PDC takes values between $[0, 1]$ because of the normalization criterion. It displays direct channel flows, and unlike the DTF, it is normalized to provide a ratio of outflows from channel v^{th} to channel u^{th} to total outflows from the source channel v^{th}, emphasizing sinks rather than sources. The observed flow intensities are influenced by PDC normalization [45].

5) Synchronization Likelihood (SL): Synchronization likelihood (SL) [30] is a widely used metric for estimating generalized synchronization in neurophysiological data, and it is strongly connected to the idea of generalized mutual information [46]. It focuses on identifying concurrent patterns to provide a normalized approximation of the dynamical inter-dependencies between multiple time series. As a result, SL is a true multivariate system. Consider M time series $x_1(t), \ldots, x_M(t)$. Embedded vectors $X_{p,t1}$ are reconstructed from each time series and represented in Eq. (8).

$$X_{p,t_1} = (x_{p,t_1}, x_{p,t_1+l}, x_{p,t_1+2l}, \ldots, x_{p,t_1+(d-1)l}) \tag{8}$$

Here, p varies from 1 to M (channel number), t_1 varies from 1 to N (discrete-time), l is the lag and d is the embedding dimension. Eq. 9 presents a variable that represents the probability of two embedded vectors being closer to each other than a distance of ϵ.

$$P^{\epsilon}_{p,t_1} = \frac{1}{2(w_2 - w_1)} \sum_{t_2=1}^{N} \theta(\epsilon - |X_{p,t_1} - X_{p,t_2}|)$$
$$\text{here}, w_1 < |t_1 - t_2| < w_2 \tag{9}$$

Here, θ presents the heavy-side step function, which equals 1 for every positive input, else zero, w_1 is a window used to correct auto-correlation effects and should be the order of the auto-correlation time or more, w_2 is a window to sharpen the time resolution of the synchronization measure. Now, for each value of p and t_1, $\epsilon_{p,t1}$ the critical distance is determined for which $P^{\epsilon}_{p,t1} = p_{ref} \ll 1$. The number of channels $H_{t1,t2}$ for each discrete time pair (t_1, t_2) within our considered window $(w_1 < |t_1 - t_2| < w_2)$ and where the embedded vectors $X_{p,t1}$ and $X_{p,t2}$ will be close together than this critical distance $\epsilon_{p,t1}$ can be determined.

$$H_{t_1,t_2} = \sum_{p=1}^{M} \theta(\epsilon_{p,t_1} - |X_{p,t_1} - X_{p,t_2}|) \tag{10}$$

This value, which ranges from 0 to M, indicates how many of the embedded signals "resemble" one another. Eq. 11 defines a synchronization likelihood $S_{p,t1,t2}$ for each channel p and each discrete time pair (t_1, t_2).

$$if |X_{p,t_1} - X_{p,t_2}| < \quad \epsilon_{p,t_1} : S_{p,t_1,t_2} = \frac{H_{t_1,t_2} - 1}{M - 1} \tag{11}$$

$$if |X_{p,t_1} - X_{p,t_2}| \geq \quad \epsilon_{p,t_1} : S_{p,t_1,t_2} = 0 \tag{12}$$

Synchronization likelihood $S_{p,t1}$ is the average of all t_2,

$$S_{p,t_1} = \frac{1}{2(w_2 - w_1)} \sum_{t_2=1}^{N} S_{p,t1,t2},$$
$$\text{where, } w_1 < |t_1 - t_2| < w_2 \tag{13}$$

$S_{p,t1}$ indicates how closely channel p is synchronised to all other $M - 1$ channels at time t_1. It takes on values between p_{ref} and 1, where p_{ref} denotes that all M time series are uncorrelated and 1 denotes that all M time series are maximally synchronised.

6) Pearson's Correlation Coefficient (COR): Pearson's correlation coefficient (COR) is used to detect linear dependencies. It calculates the time-domain linear correlation between two signals $x(t)$ and $y(t)$ at zero latency [33]. It is defined as:

$$\rho_{x,y} = \frac{cov(x, y)}{\sigma_x \sigma_y} \tag{14}$$

where $\rho_{x,y}$ is the correlation coefficient between signals x and y, $\sigma x, \sigma y$ are standard deviation of x and y respectively and $cov(x, y)$ is the co-variance. Also, $-1 \leq \rho_{x,y} \leq 1$, where -1 represents complete linear inverse correlation, 0 represents no linear dependence and 1 represents complete linear dependence between the two signals.

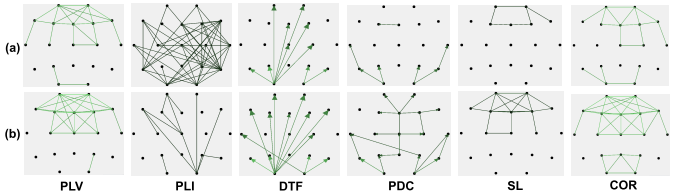

Fig. 4. Group differences as graphs for different connectivity measures including PLV, PLI, DTF, PDC, SL and COR. Here rows represent (a) Healthy patient and (b) SCZ Patient. Directions of information flow are indicated using arrows.

E. Proposed Neural Network Architectures

In the present work, five different architectures of neural networks are tested and analyzed (see Table I). A bunch of parameters are involved in designing a neural network like activation functions, loss functions, optimizers, and several neurons. All these parameters are discussed in this section.

For the hidden layers, Rectified linear unit (ReLU) is applied as the activation function. ReLU is amongst the simplest and conventionally used of all activation functions. ReLU does not saturate for large input values, unlike other conventional activation functions, and returns zero as output if the input to it is a negative or zero, but for all positive input values, it returns the number itself [47]. This helps the model train quickly, achieve high accuracy and overcome the vanishing gradient problem, allowing the model to learn faster [48]. It can be simply defined as, $y = \max(0, x)$, where, x and y are input and output, respectively. For the output layer, we use Softmax as the activation function due to its ability to convert a vector of numbers to a vector of probabilities. It is configured to output n values, where n is the number of classes, and also helps normalize these values. Each value in the output is interpreted as a probability; thus, the sum of all output values equals 1 [47], [49]. It can be defined as, $\sigma(z_i) = \frac{e^{\vec{z_i}}}{\sum_{j=1}^{n} e^{\vec{z_i}}}$, Here, $\vec{z}$ is the input vector, and n is the number of classes in our classifier. We use Binary cross-entropy as the loss function in our neural network architectures. It can be mathematically defined as, $\text{loss} = \frac{1}{N}\sum_{i=1}^{N} -((y_i)\cdot\log(p_i)+(1-y_i)\cdot\log(1-p_i))$, where y_i is the actual output value and p_i is the probability of output 1. Adam is used as the optimizer due to its ability to achieve results faster than other optimizers [50]. The final results are obtained after averaging over 50 iterations of Monte Carlo cross-validation along with stratification [51]. Architecture-1 contains 2 layers. The single hidden layer contains 2 neurons with ReLU activation function, and the output layer has a Softmax activation function. Similarly, Architecture-2, 3, and 4 contain a single hidden layer with 4, 16, and 32 neurons, respectively. Architecture 5 consists of 2 hidden layers with 16 and 32 neurons, respectively.

F. Multimodal Late Fusion Technique

The brain is a complex organ, and to analyze brain networks effectively, there is a need to look at it from various viewpoints. The above-discussed connectivity measures can help to do that, but it can be taken a step further, i.e., making use of latent features derived from the fusion of all six connectivity measures in a particular manner [27], [52]. In the present work, a multimodal fusion technique known as "Late Fusion"

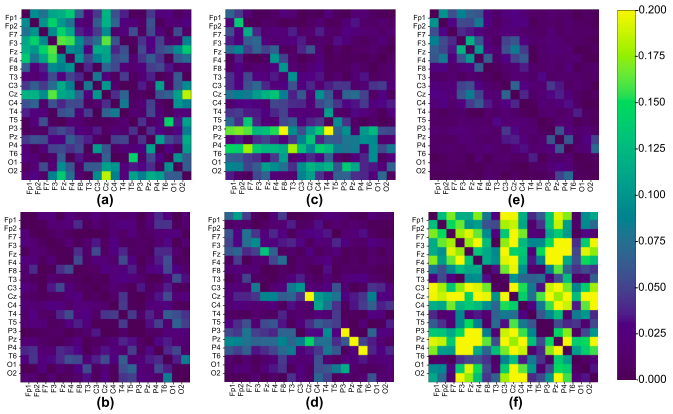

Fig. 5. Difference in average adjacency matrices of (a) PLV, (b) PLI, (c) DTF, (d) PDC, (e) SL, (f) COR connectivity methods, shown in the form of an adjacency matrix.

is performed. The structure of this fusion technique is shown in Fig. 3. Here, independent neural networks are trained for individual connectivity feature domains, and the prediction probabilities from the softmax layer of all the domain-specific neural networks are then combined to give a single final prediction. The layer-wise overview of neural network model architectures 1-5 is shown in Fig. 2. The main reason for using the fusion technique was to effectively combine the Phase Synchronization, Causality, and Correlation measures and input the same as a multimodal input feature.

G. Evaluation Metrics

Confusion-matrix based evaluation was used to access the performance of the proposed method [53]. In addition to the confusion matrix-based evaluation metric, ROC curves were also used to evaluate model performance [54]. The same has been discussed in detail in the supplementary materials.

III. Results and Discussion

Performance of the various neural network architectures in classifying SCZ and non-SCZ samples using brain connectivity measures is evaluated. We used the SCZ EEG dataset [34], open-sourced by the Institute of Psychiatry and Neurology in Warsaw, Poland. The dataset consists of EEG signals from 14 healthy and 14 SCZ subjects. The resting-state EEG signals were recorded with a sampling frequency of 250Hz from 19 channels (Fp1, Fp2, F7, F3, Fz, F4, F8, T3, C3, Cz, C4, T4, T5, P3, Pz, P4, T6, O1, and O2). The adjacency matrices and the connectivity graphs are calculated using HERMES Toolbox [41] based on MATLAB. This toolbox specifically studies the functionality and effectiveness of brain connectivity and provides visualizations to analyze the group difference between different classes. Neural network architectures were trained using conventional sequential training. This includes training epochs = 50, learning rate = 0.001 and Adam as the optimizer. In place of dropout, early stopping was used to avoid overfitting (with min_delta = 0 and patience = 10, monitoring "val_accuracy"). Experiments were performed on an Intel Core i5 (5th Gen) system with a 1.6 GHz processor and 8GB DDR4 RAM running Linux (Ubuntu 20.04).

The EEG signals within the frequencies of the alpha band (8-12.5 Hz) [37] are analyzed. A comparison is made among

TABLE I
CLASSIFICATION PERFORMANCE COMPARISON OF DIFFERENT NEURAL NETWORK ARCHITECTURES ON THE SIX CONNECTIVITY MEASURES

Connectivity methods	Arch.	Training Accuracy	Validation Accuracy	Test Accuracy	Precision	Recall
PLV	1	80.32	78.91	81.10	73.35	84.98
	2	86.06	85.19	87.22	84.19	92.30
	3	98.06	97.94	99.11	99.00	99.25
	4	97.74	98.02	99.44	99.04	99.86
	5	98.66	98.18	99.86	99.73	100.00
PLI	1	78.75	76.52	77.69	78.69	75.76
	2	83.52	82.89	84.38	83.75	86.13
	3	90.42	87.68	89.76	89.48	90.54
	4	93.78	90.70	92.15	92.38	92.10
	5	96.80	93.14	94.18	93.57	95.11
DTF	1	92.39	91.61	93.40	90.05	93.79
	2	98.51	98.22	99.52	99.29	99.79
	3	98.92	98.78	99.96	100.00	99.93
	4	98.68	98.73	99.98	100.00	99.96
	5	98.56	98.59	100.00	100.00	100.00
PDC	1	92.52	91.75	94.16	93.95	99.45
	2	96.71	96.85	98.44	97.44	97.45
	3	98.44	98.36	99.91	100.00	99.83
	4	98.49	98.78	99.98	100.00	99.96
	5	98.57	98.52	100.00	100.00	100.00
SL	1	73.30	72.47	75.57	67.80	75.32
	2	79.60	78.26	82.79	76.46	80.50
	3	91.98	92.43	95.10	94.66	95.79
	4	95.61	94.91	97.37	97.48	97.28
	5	98.05	97.36	99.18	98.84	99.55
COR	1	93.24	92.66	94.88	93.73	98.23
	2	95.36	95.08	97.03	95.50	95.62
	3	98.48	98.68	99.84	99.70	100.00
	4	98.34	98.28	99.94	99.90	100.00
	5	98.24	98.42	100.00	100.00	100.00

the six connectivity measures and the five neural network architectures. The results are obtained after performing Monte Carlo cross-validation along with stratification. stratification was performed to ensure that in those random splits, the ratio of healthy to SCZ remained consistent. Thus, all the metric values are obtained by averaging over all 50 Monte Carlo iterations. For each of the 50 iterations, the samples were split randomly in a ratio of 70% training set, 15% validation set, and 15% test set. During implementation, a constant random seed generator was fixed in the study in the Jupyter Notebook and all results were reported after 50-fold cross-validation. Table I shows a comparison of the classification performance of all five neural network architectures on the six connectivity methods. It is possible to observe that in the case of PLV, the average training accuracy for Architecture 1 is at 80.32%, and it keeps increasing proportionally with a more significant number of neurons and hidden layers used by the other architectures. One crucial thing to observe here is that the training accuracy increases significantly until Architecture 3 and then stagnates. A similar trend is observed for the other evaluation metrics. It is a familiar fact that increasing the number of neurons or the hidden layers in a neural network can help extract more features from the input data, but it happens only to a certain extent. There is always a limit that is dependent on the size of our input features. Increasing the number of neurons/layers above that limit can result in over-fitting and thus reduce the classification accuracies. The stagnation in accuracy above Architecture 3 indicates that we are very close to that limit corresponding to our dataset. The results associated with the late fusion methodology are shown in Table II. It is interesting to note that Architecture 5 gives a slightly lower accuracy than Architecture 4. Here, it is very likely that the same reasoning will follow.

TABLE II
CLASSIFICATION PERFORMANCE OF LATE FUSION

Architectures	Accuracy	Precision	Recall
1	88.95	81.73	78.13
2	94.76	92.96	90.77
3	99.63	99.63	99.62
4	99.84	99.86	99.83
5	98.75	97.95	99.76

The ROC curve diagram for Architectures 1-5 for all six connectivity methods is shown in the supplementary material. Each graph contains ROC curves for all 50 Monte Carlo iterations. Here, the area under the curve (AUC) measures a classifier's ability to differentiate classes. A model with the highest AUC best differentiates between positive and negative classes. It is observed that the model improves over subsequent iterations, and also, the high number of diagonal curves for architecture 1, as compared to architectures 3 and 5, are very apparent. That is, the AUC is lower for architecture one than for architecture 3 and 5, which validates the trend observed.

Group differences for each connectivity measure are shown as graphs (see Fig. 4). Here, only the strongest connections are illustrated. For PLV, the calculations were performed at a threshold of 70, implying that only 30% of the strongest connections were considered. Similarly, 84%, 60%, 70%, 80%, and 40% of the strongest linkages were considered for PLI, DTF, PDC, SL, and COR, respectively. Increasing the threshold by ten signifies that 10% of the weakest connections were removed. Since the network is strongly linked, removing even 90% of the weakest links does not fully alter the typical connectivity pattern. Statistically significant differences were observed between various groups. Among the different connectivity methods, it is possible to observe that the best results are associated with the models trained with the adjacency matrices of DTF and PDC models. According to this, evidence suggests that the causality connectivity methods can deliver richer information that can be used to build classification models compared to the phase synchronization connectivity methods. In contrast to PLV and PLI, directionality measures like DTF allowed for identifying the key drivers and directions of information flow. There were more flows from the posterior to the frontal brain areas in SCZ patients, which can also be seen in Fig. 4. The increased number of flows corresponds to a stronger PLV in frontal brain regions, also seen in the obtained connectivity graphs. The EEG data collected under resting-state settings with eyes open and closed has previously revealed connections between PLV and DTF [55]. The strength and area of synchronization also depend on the method used to measure it. From Fig. 4, it is observed that in patients diagnosed with SCZ, frontal brain regions are more synchronized as depicted by PLV and PLI shows us a weaker synchronization in the posterior areas. Synchronization, quantified by PLV, was observed to be high in SCZ patients in contrast to

TABLE III
PERFORMANCE COMPARISON OF SCHIZO-NET WITH STATE-OF-THE-ART MODELS WHICH WERE TRAINED ON THE SAME DATASET

Works	Year	Computed features	Classification Method	Classification Accuracy
Oh et al. [20]	2019	Automated feature extraction	Deep CNN	98.07% (non-subject)/81.26% (subject)
Jahmunah et al. [21]	2019	Non-linear feature mining	Decision Tree, SVM, LDA, Probabilistic-NN, kNN	92.91% (SVM)
Buettner et al. [64]	2019	ICA, FFT	Random Forest	80.00%
Racz et al. [65]	2020	Graph theoretical analysis based	Random Forest	89.29%
Krishnan et al. [66]	2020	Approximate entropy, Sample entropy, Permutation entropy, Spectral entropy, Singular Value Decomposition entropy	SVM	93.00%
Buettner et al. [67]	2020	Mean over all sensors, Spectral Analysis	Random Forest	96.77%
Aslan and Akin [68]	2020	Automated Feature Extraction	VGG-16 Transfer Learning	97%
Singh et al. [69]	2020	EEG band are separated using FFT spectrum; several features are extracted	Deep CNN	98.56%
Chandran et al. [70]	2020	Nonlinear feature extraction	LSTM	99.10%
Das and Pachori [71]	2021	Hjorth features	SVM (Cubic)	98.90%
Schizo-Net	2022	Brain connectivity measures	DNN	**99.84%** (Arch-IV) with late fusion

TABLE IV
PERFORMANCE COMPARISON OF SCHIZO-NET WITH OTHER STATE-OF-THE-ART TECHNIQUES IN SCZ LITERATURE

Works	Year	EEG dataset	Computed features	Classification Method	Classification Accuracy
Sabeti et al. [56]	2007	SCZ: 20; Control: 20	Autoregressive model parameters, band power, fractal dimension, wavelet energy	LDA, SVM	88.23% (LDA) and 99.54% (SVM)
Sabeti et al. [58]	2011	SCZ: 20; Control: 20	Autoregressive parameters, band power, fractal dimension	LDA, Adaboost	85.90% (LDA) and 91.94% (Adaboost)
Johannesen et al. [59]	2016	SCZ: 40; control: 12	Five frequency band based parameters	SVM	87.00%
Thilakvathi et al. [57]	2017	SCZ: 55; control: 23	Entropies, fractal dimension, Kolmogorov complexity	SVM	88.50%
Phang et al. [27]	2019	SCZ: 45; control: 39	Vector-auto regression based directed connectivity, graph-theoretical complex network	DNN	95.00%
Devia et al. [60]	2019	SCZ: 11; control: 9	Event Related Potentials (ERPs) features	LDA	71.00%
Siuly et al. [18]	2020	SCZ: 49; control: 32	Empirical mode decomposition based characteristics	Ensemble bagged tree	89.59%
Schizo-Net	2022	SCZ: 14; control: 14	Brain connectivity measures	DNN	**99.84%** (Arch-IV) with late fusion

non-SCZ counterparts. Moreover, reduced information flows in the frontal part of the brain but increased flows from the occipital lobe to the frontal brain lobe were observed. The differences in average adjacency matrices for subjects diagnosed with SCZ and the control set of non-SCZ individuals are shown in Fig. 5. This provides insights into the degree to which each connectivity method helps us distinguish between the two classes. The differences in PLI and SL adjacency matrices are very scarce, complying with their low classification accuracy. These adjacency matrices are calculated for the six connectivity measures. Tables III and IV shows the performance comparison of Schizo-Net with state-of-the-art techniques in the current SCZ literature.

IV. CONCLUSION AND FUTURE WORK

The study presents *Schizo-Net*, a novel method of utilizing brain connectivity methods to diagnose schizophrenia from Electroencephalogram (EEG) signals. The significance of this approach for SCZ detection is demonstrated experimentally by comparing six connectivity measures reflecting different brain connectivity aspects, namely PLV, PDC, PLI, COR, DTF, and SL. Each metric conveys information about the interactions within and between brain areas in a distinct way. These measurements reveal crucial characteristics such as correlation, phase synchronization, and directional information flow between different brain areas. They support the examination of the neural mechanisms underlying disconnectivity disorders. Here, shallow neural networks are showing decent accuracy. The present study provides an efficient and reliable method for diagnosing SCZ using the concept of brain connectivity. We achieved state-of-the-art accuracy (of 99.84%) for different measures using deep neural networks. Monte Carlo cross-validation along with stratification was performed to validate the obtained results. The contribution of the present study is that the classification based on connectivity features is successful primarily due to the effective deep learning-based processing of brain connectivity indices associated with SCZ. The study has a few limitations. First, only alpha bands have been considered while designing the diagnosis model. Even though it has been established that alpha bands are advantageous compared to other bands in differentiating SCZ patients from control, it would be interesting to see how deep learning models perform on other bands in future studies. Second, all neural network models have been given equal weightage in late fusion. What would be ideal is to give

more weightage to the connectivity feature that performs better classification. Future studies can focus on designing the weighted distribution of late fusion prediction. Future studies can also focus on expanding *Schizo-Net* with the notions of explainability, deep-precognitive diagnosis [63], and other disorders like myocardial infarction [73], [74].

REFERENCES

[1] M. J. Owen, A. Sawa, and P. B. Mortensen, "Schizophrenia," *Lancet*, vol. 388, no. 10039, pp. 86–97, 2016, doi: 10.1016/S0140-6736(15)01121-6.

[2] *American Psychiatric Association, Diagnostic and statistical Manual of Mental Disorders: DSM-5*, 5th ed. Arlington, TX, USA: American Psychiatric Association Publishing, 2013, doi: 10.1176/appi.books.9780890425596.

[3] A. Schmitt, A. Hasan, O. Gruber, and P. Falkai, "Schizophrenia as a disorder of disconnectivity," *Eur. Arch. Psychiatry Clin. Neurosci.*, vol. 261, no. S2, pp. 150–154, Nov. 2011, doi: 10.1007/s00406-011-0242-2.

[4] E. Johnstone, C. D. Frith, T. J. Crow, J. Husband, and L. Kreel, "Cerebral ventricular size and cognitive impairment in chronic schizophrenia," *Lancet*, vol. 308, no. 7992, pp. 924–926, 1976, doi: 10.1016/s0140-6736(76)90890-4.

[5] *Mental Illness Hospitals and Units in England: Schizophrenia Statistics 1981–88*, Dept. Health Social Secur., London, U.K., 1986.

[6] J. H. Boyd, A. E. Pulver, and W. Stewart, "Season of birth: Schizophrenia and bipolar disorder," *Schizophr. Bull.*, vol. 12, no. 2, pp. 173–186, 1986, doi: 10.1093/schbul/12.2.173.

[7] R. A. Machón, S. A. Mednick, and F. Schulsinger, "Seasonality, birth complications and schizophrenia in a high risk sample," *Br. J. Psychiatry*, vol. 151, no. 1, pp. 122–124, 1987, doi: 10.1192/bjp.151.1.122.

[8] T. Videbech, A. Weeke, and A. Dupont, "Endogenous psychoses and season of birth," *Acta Psychiatrica Scandinavica*, vol. 50, no. 2, pp. 202–218, Apr. 1974, doi: 10.1111/j.1600-0447.1974.tb08209.x.

[9] M. E. Shenton, C. C. Dickey, M. Frumin, and R. W. McCarley, "A review of MRI findings in schizophrenia," *Schizophr. Res.*, vol. 49, nos. 1–2, pp. 1–52, 2001, doi: 10.1016/s0920-9964(01)00163-3.

[10] C.-R. Phang, F. Noman, H. Hussain, C.-M. Ting, and H. Ombao, "A multi-domain connectome convolutional neural network for identifying schizophrenia from EEG connectivity patterns," *IEEE J. Biomed. Health Informat.*, vol. 24, no. 5, pp. 1333–1343, May 2020, doi: 10.1109/JBHI.2019.2941222.

[11] *Schizophrenia*. Accessed: Mar. 10, 2022. [Online]. Available: https://www.who.int/news-room/fact-sheets/detail/schizophrenia

[12] C. Hua, H. Wang, J. Chen, T. Zhang, Q. Wang, and W. Chang, "Novel functional brain network methods based on CNN with an application in proficiency evaluation," *Neurocomputing*, vol. 359, pp. 153–162, Sep. 2019, doi: 10.1016/j.neucom.2019.05.088.

[13] M. B. T. Noor, N. Z. Zenia, M. S. Kaiser, S. A. Mamun, and M. Mahmud, "Application of deep learning in detecting neurological disorders from magnetic resonance images: A survey on the detection of Alzheimer's disease, Parkinson's disease and schizophrenia," *Brain Inform.*, vol. 7, no. 1, p. 11, 2020, doi: 10.1186/s40708-020-00112-2.

[14] M. A. Berg, A. M. Morrow, and M. C. Hout, "Wake up, brain!: Using electricity to think and feel differently," *Frontiers Young Minds*, vol. 7, pp. 1–9, May 2019, doi: 10.3389/frym.2019.00062.

[15] K. Kotowski, K. Stapor, and J. Ochab, "Deep learning methods in electroencephalography," in *Learning and Analytics in Intelligent Systems*. Cham, Switzerland: Springer, 2020, pp. 191–212.

[16] R. Upadhyay, P. K. Padhy, and P. K. Kankar, "Ocular artifact removal from EEG signals using discrete orthonormal stockwell transform," in *Proc. Annu. IEEE India Conf. (INDICON)*, Dec. 2015, pp. 1–5, doi: 10.1109/INDICON.2015.7443617.

[17] S. Kumari, R. Upadhyay, P. K. Padhy, and P. K. Kankar, "Application of empirical mode decomposition for feature extraction from EEG signals," in *Proc. Int. Conf. Comput., Commun. Control (IC)*, Sep. 2015, pp. 1-6, doi: 10.1109/IC4.2015.7375508.

[18] S. Siuly, S. K. Khare, V. Bajaj, H. Wang, and Y. Zhang, "A computerized method for automatic detection of schizophrenia using EEG signals," *IEEE Trans. Neural Syst. Rehabil. Eng.*, vol. 28, no. 11, pp. 2390–2400, Nov. 2020, doi: 10.1109/TNSRE.2020.3022715.

[19] S. K. Khare, V. Bajaj, and U. R. Acharya, "SPWVD-CNN for automated detection of schizophrenia patients using EEG signals," *IEEE Trans. Instrum. Meas.*, vol. 70, pp. 1–9, 2021, doi: 10.1109/TIM.2021.3070608.

[20] S. L. Oh, J. Vicnesh, E. J. Ciaccio, R. Yuvaraj, and U. R. Acharya, "Deep convolutional neural network model for automated diagnosis of schizophrenia using EEG signals," *Appl. Sci.*, vol. 9, no. 14, p. 2870, 2019, doi: 10.3390/app9142870.

[21] V. Jahmunah et al., "Automated detection of schizophrenia using nonlinear signal processing methods," *Artif. Intell. Med.*, vol. 100, Sep. 2019, Art. no. 101698, doi: 10.1016/j.artmed.2019.07.006.

[22] N. Zhou and L. Wang, "A modified T-test feature selection method and its application on the HapMap genotype data," *Genomics, Proteomics Bioinf.*, vol. 5, no. 3, pp. 242–249, 2007, doi: 10.1016/S1672-0229(08)60011-X.

[23] Z. Dvey-Aharon, N. Fogelson, A. Peled, and N. Intrator, "Schizophrenia detection and classification by advanced analysis of EEG recordings using a single electrode approach," *PLoS ONE*, vol. 10, no. 4, Apr. 2015, Art. no. e0123033, doi: 10.1371/journal.pone.0123033.

[24] A. E. Hramov, N. S. Frolov, V. A. Maksimenko, S. A. Kurkin, V. B. Kazantsev, and A. N. Pisarchik, "Functional networks of the brain: From connectivity restoration to dynamic integration," *Physics-Uspekhi*, vol. 64, no. 6, pp. 584–616, Sep. 2021, doi: 10.3367/UFNe.2020.06.038807.

[25] G. Chen, G. Chen, C. Xie, and S.-J. Li, "Negative functional connectivity and its dependence on the shortest path length of positive network in the resting-state human brain," *Brain Connectivity*, vol. 1, no. 3, pp. 195–206, 2011, doi: 10.1089/brain.2011.0025.

[26] S.-E. Moon, C.-J. Chen, C.-J. Hsieh, J.-L. Wang, and J.-S. Lee, "Emotional EEG classification using connectivity features and convolutional neural networks," *Neural Netw.*, vol. 132, pp. 96–107, Dec. 2020, doi: 10.1016/j.neunet.2020.08.009.

[27] C.-R. Phang, C.-M. Ting, S. B. Samdin, and H. Ombao, "Classification of EEG-based effective brain connectivity in schizophrenia using deep neural networks," in *Proc. 9th Int. IEEE/EMBS Conf. Neural Eng. (NER)*, Mar. 2019, pp. 401–406, doi: 10.1109/NER.2019.8717087.

[28] J. P. Lachaux, E. Rodriguez, J. Martinerie, and F. J. Varela, "Measuring phase synchrony in brain signals," *Hum. Brain Mapping*, vol. 8, no. 4, pp. 194–208, Jan. 1999, doi: 10.1002/(SICI)1097-0193(1999)8:4%3C194:AID-HBM4%3E3.0.CO;2-C.

[29] C.J. Stam, G. Nolte, and A. Daffertshofer, "Phase lag index: Assessment of functional connectivity from multi channel EEG and MEG with diminished bias from common sources," *Hum. Brain Mapping.*, vol. 28, no. 11, pp. 1178–1193, Nov. 2007, doi: 10.1002/hbm.20346.

[30] C. J. Stam and B. W. van Dijk, "Synchronization likelihood: An unbiased measure of generalized synchronization in multivariate data sets," *Phys. D, Nonlinear Phenomena*, vol. 163, nos. 3–4, pp. 236–251, 2002, doi: 10.1016/S0167-2789(01)00386-4.

[31] M. Kamiński, M. Ding, W. A. Truccolo, and S. L. Bressler, "Evaluating causal relations in neural systems: Granger causality, directed transfer function and statistical assessment of significance," *Biol. Cybern.*, vol. 85, no. 2, pp. 145–157, Aug. 2001, doi: 10.1007/s004220000235.

[32] L. A. Baccalá and K. Sameshima, "Partial directed coherence: A new concept in neural structure determination," *Biol. Cybern.*, vol. 84, no. 6, pp. 463–474, May 2001, doi: 10.1007/PL00007990.

[33] G. Nahler, "Pearson correlation coefficient," in *Dictionary of Pharmaceutical Medicine*. Vienna, Austria: Springer, 2009, p. 132, doi: 10.1007/978-3-211-89836-9_304.

[34] E. Olejarczyk and W. Jernajczyk, "Graph-based analysis of brain connectivity in schizophrenia," *PLoS ONE*, vol. 12, no. 11, Nov. 2017, Art. no. e0188629, doi: 10.1371/journal.pone.0188629.

[35] R. Upadhyay, P. K. Kankar, P. K. Padhy, and V. K. Gupta, "Extraction and classification of electroencephalogram signals," in *Proc. IEEE Int. Conf. Comput. Intell. Comput. Res.*, Dec. 2012, pp. 1–4.

[36] A. Delorme and S. Makeig, "EEGLAB: An open source toolbox for analysis of single-trial EEG dynamics including independent component analysis," *J. Neurosci. Methods*, vol. 134, no. 1, pp. 9–21, Mar. 2004, doi: 10.1016/j.jneumeth.2003.10.009.

[37] A. Fink, R. H. Grabner, C. Neuper, and A. C. Neubauer, "EEG alpha band dissociation with increasing task demands," *Cognit. Brain Res.*, vol. 24, no. 2, pp. 252–259, Jul. 2005, doi: 10.1016/j.cogbrainres.2005.02.002.

[38] C.-Y. Chang, S.-H. Hsu, L. Pion-Tonachini, and T.-P. Jung, "Evaluation of artifact subspace reconstruction for automatic EEG artifact removal," in *Proc. 40th Annu. Int. Conf. IEEE Eng. Med. Biol. Soc. (EMBC)*, Jul. 2018, pp. 1242–1245, doi: 10.1109/EMBC.2018.8512547.

[39] P. Comon. (1992). *Independent Component Analysis*. Higher-Order Statistics. Accessed: Mar. 10, 2022. [Online]. Available: https://hal.archives-ouvertes.fr/hal-00346684/

[40] E. S. Juan et al., "Comparison between FastICA and InfoMax for the blind separation of audio signals," in *Proc. 11th Int. Symp. Commun. Syst., Netw. Digit. Signal Process. (CSNDSP)*, 2018, pp. 1–4.

[41] G. Niso et al., "HERMES: Towards an integrated toolbox to characterize functional and effective brain connectivity," *Neuroinformatics*, vol. 11, no. 4, pp. 405–434, 2013, doi: 10.1007/s12021-013-9186-1.

[42] F. Mormann, K. Lehnertz, P. David, and C. E. Elger, "Mean phase coherence as a measure for phase synchronization and its application to the EEG of epilepsy patients," *Phys. D, Nonlinear Phenomena*, vol. 144, nos. 3–4, pp. 358–369, 2000, doi: 10.1016/S0167-2789(00)00087-7.

[43] S. P. van den Broek, F. Reinders, M. Donderwinkel, and M. J. Peters, "Volume conduction effects in EEG and MEG," *Electroencephalogr. Clin. Neurophysiol.*, vol. 106, no. 6, pp. 522–534, 1998, doi: 10.1016/S0013-4694(97)00147-8.

[44] M. Eichler, "On the evaluation of information flow in multivariate systems by the directed transfer function," *Biol. Cybern.*, vol. 94, no. 6, pp. 469–482, Jun. 2006, doi: 10.1007/s00422-006-0062-z.

[45] B. Schelter, J. Timmer, and M. Eichler, "Assessing the strength of directed influences among neural signals using renormalized partial directed coherence," *J. Neurosci. Methods*, vol. 179, no. 1, pp. 121–130, Apr. 2009, doi: 10.1016/j.jneumeth.2009.01.006.

[46] T. Buzug, K. Pawelzik, J. von Stamm, and G. Pfister, "Mutual information and global strange attractors in Taylor-Couette flow," *Physica D, Nonlinear Phenomena*, vol. 72, no. 4, pp. 343–350, 1994, doi: 10.1016/0167-2789(94)90237-2.

[47] B. Asadi and H. Jiang, "On approximation capabilities of ReLU activation and softmax output layer in neural networks," 2020, *arXiv:2002.04060*.

[48] A. M. Javid, S. Das, M. Skoglund, and S. Chatterjee, "A ReLU dense layer to improve the performance of neural networks," in *Proc. IEEE Int. Conf. Acoust., Speech Signal Process. (ICASSP)*, Jun. 2021, pp. 2810–2814.

[49] O. Sharma, "A new activation function for deep neural network," in *Proc. Int. Conf. Mach. Learn., Big Data, Cloud Parallel Comput. (COMITCon)*, Feb. 2019, pp. 84–86.

[50] D. P. Kingma and J. Ba, "Adam: A method for stochastic optimization," 2014, *arXiv:1412.6980*.

[51] Q.-S. Xu and Y.-Z. Liang, "Monte Carlo cross validation," *Chemometrics Intell. Lab. Syst.*, vol. 56, no. 1, pp. 1–11, 2001, doi: 10.1016/S0169-7439(00)00122-2.

[52] Y. Dong, S. Gao, K. Tao, J. Liu, and H. Wang, "Performance evaluation of early and late fusion methods for generic semantics indexing," *Pattern Anal. Appl.*, vol. 17, no. 1, pp. 37–50, Feb. 2014, doi: 10.1007/s10044-013-0336-8.

[53] M. Hossin and M. N. Sulaiman, "A review on evaluation metrics for data classification evaluations," *Int. J. Data Mining Knowl. Manage. Process*, vol. 5, no. 2, pp. 1–11, Mar. 2015, doi: 10.5121/ijdkp.2015.5201.

[54] K. H. Zou, A. J. O'Malley, and L. Mauri, "Receiver-operating characteristic analysis for evaluating diagnostic tests and predictive models," *Circulation*, vol. 115, no. 5, pp. 654–657, Feb. 2007, doi: 10.1161/CIRCULATIONAHA.105.594929.

[55] E. Olejarczyk, L. Marzetti, V. Pizzella, and F. Zappasodi, "Comparison of connectivity analyses for resting state EEG data," *J. Neural Eng.*, vol. 14, no. 3, Jun. 2017, Art. no. 036017, doi: 10.1088/1741-2552/aa6401.

[56] M. Sabeti, R. Boostani, S. D. Katebi, and G. W. Price, "Selection of relevant features for EEG signal classification of schizophrenic patients," *Biomed. Signal Process. Control*, vol. 2, no. 2, pp. 122–134, Apr. 2007, doi: 10.1016/j.bspc.2007.03.003.

[57] B. Thilakvathi, K. Bhanu, and M. Malaippan, "EEG signal complexity analysis for schizophrenia during rest and mental activity," *Biomed. Res.*, vol. 28, pp. 1–9, Jan. 2017.

[58] M. Sabeti, S. D. Katebi, R. Boostani, and G. W. Price, "A new approach for EEG signal classification of schizophrenic and control participants," *Expert Syst. Appl.*, vol. 38, no. 3, pp. 2063–2071, 2011, doi: 10.1016/j.eswa.2010.07.145.

[59] J. K. Johannesen, J. Bi, R. Jiang, J. G. Kenney, and C.-M.-A. Chen, "Machine learning identification of EEG features predicting working memory performance in schizophrenia and healthy adults," *Neuropsychiatric Electrophysiol.*, vol. 2, no. 1, pp. 1–21, Dec. 2016, doi: 10.1186/s40810-016-0017-0.

[60] C. Devia et al., "EEG classification during scene free-viewing for schizophrenia detection," *IEEE Trans. Neural Syst. Rehabil. Eng.*, vol. 27, no. 6, pp. 1193–1199, Apr. 2019, doi: 10.1109/TNSRE.2019.2913799.

[61] A. V. Chikkankod and L. Longo, "On the dimensionality and utility of convolutional Autoencoder's latent space trained with topology-preserving spectral EEG head-maps," *Mach. Learn. Knowl. Extraction*, vol. 4, no. 4, pp. 1042–1064, Nov. 2022, doi: 10.3390/make4040053.

[62] L. Longo, "Modeling cognitive load as a self-supervised brain rate with electroencephalography and deep learning," *Brain Sci.*, vol. 12, no. 10, p. 1416, Oct. 2022, doi: 10.3390/brainsci12101416.

[63] A. Chharia et al., "Deep-precognitive diagnosis: Preventing future pandemics by novel disease detection with biologically-inspired conv-fuzzy network," *IEEE Access*, vol. 10, pp. 23167–23185, 2022, doi: 10.1109/ACCESS.2022.3153059.

[64] R. Buettner, M. Hirschmiller, K. Schlosser, M. Rossle, M. Fernandes, and I. J. Timm, "High-performance exclusion of schizophrenia using a novel machine learning method on EEG data," in *Proc. IEEE Int. Conf. E-Health Netw., Appl. Services (HealthCom)*, Oct. 2019, pp. 1–6.

[65] F. S. Racz, O. Stylianou, P. Mukli, and A. Eke, "Multifractal and entropy-based analysis of delta band neural activity reveals altered functional connectivity dynamics in schizophrenia," *Frontiers Syst. Neurosci.*, vol. 14, p. 49, Jul. 2020, doi: 10.3389/fnsys.2020.00049.

[66] P. T. Krishnan, A. N. J. Raj, P. Balasubramanian, and Y. Chen, "Schizophrenia detection using MultivariateEmpirical mode decomposition and entropy measures from multichannel EEG signal," *Biocybernetics Biomed. Eng.*, vol. 40, no. 3, pp. 1124–1139, Jul. 2020, doi: 10.1016/j.bbe.2020.05.008.

[67] R. Buettner, D. Beil, S. Scholtz, and A. Djemai, "Development of a machine learning based algorithm to accurately detect schizophrenia based on one-minute EEG recordings," in *Proc. Annu. Hawaii Int. Conf. Syst. Sci.*, 2020, pp. 1–10. [Online]. Available: https://scholarspace.manoa.hawaii.edu/handle/10125/64135

[68] Z. Aslan and M. Akin, "Automatic detection of schizophrenia by applying deep learning over spectrogram images of EEG signals," *Traitement du Signal*, vol. 37, no. 2, pp. 235–244, Apr. 2020, doi: 10.18280/ts.370209.

[69] K. Singh, S. Singh, and J. Malhotra, "Spectral features based convolutional neural network for accurate and prompt identification of schizophrenic patients," *Proc. Inst. Mech. Eng., H, J. Eng. Med.*, vol. 235, no. 2, pp. 167–184, Feb. 2021, doi: 10.1177/0954411920966937.

[70] A. Nikhil Chandran, K. Sreekumar, and D. P. Subha, "EEG-based automated detection of schizophrenia using long short-term memory (LSTM) network," in *Algorithms for Intelligent Systems*. Singapore: Springer, 2021, pp. 229–236.

[71] K. Das and R. B. Pachori, "Schizophrenia detection technique using multivariate iterative filtering and multichannel EEG signals," *Biomed. Signal Process. Control*, vol. 67, May 2021, Art. no. 102525, doi: 10.1016/j.bspc.2021.102525.

[72] A. Mognon, J. Jovicich, L. Bruzzone, and M. Buiatti, "ADJUST: An automatic EEG artifact detector based on the joint use of spatial and temporal features: Automatic spatio-temporal EEG artifact detection," *Psychophysiology*, vol. 48, no. 2, pp. 229–240, Feb. 2011, doi: 10.1111/j.1469-8986.2010.01061.x.

[73] S. Madhavan, R. K. Tripathy, and R. B. Pachori, "Time-frequency domain deep convolutional neural network for the classification of focal and non-focal EEG signals," *IEEE Sensors J.*, vol. 20, no. 6, pp. 3078–3086, Mar. 2020, doi: 10.1109/jsen.2019.2956072.

[74] R. K. Tripathy, A. Bhattacharyya, and R. B. Pachori, "Localization of myocardial infarction from multi-lead ecg signals using multiscale analysis and convolutional neural network," *IEEE Sensors J.*, vol. 19, no. 23, pp. 11437–11448, Dec. 2019, doi: 10.1109/jsen.2019.2935552.

[75] K. Jindal, R. Upadhyay, P. K. Padhy, and L. Longo, "Bi-LSTM-deep CNN for schizophrenia detection using MSST-spectral images of EEG signals," in *Artificial Intelligence-Based Brain-Computer Interface*, New York, NY, USA: Academic, 2022, pp. 145–162, ch. 6, doi: 10.1016/B978-0-323-91197-9.00011-4.

[76] C. Gómez-Tapia, B. Bozic, and L. Longo, "On the minimal amount of EEG data required for learning distinctive human features for task-dependent biometric applications," *Frontiers Neuroinform.*, vol. 16, May 2022, Art. no. 844667, doi: 10.3389/fninf.2022.844667.

[77] B. Raufi and L. Longo, "An evaluation of the EEG alpha-to-theta and theta-to-alpha band ratios as indexes of mental workload," *Frontiers in Neuroinformatics*, vol. 16, May 2022, Art. no. 861967, doi: 10.3389/fninf.2022.861967.

[78] T. Ahmed and L. Longo, "Examining the size of the latent space of convolutional variational autoencoders trained with spectral topographic maps of EEG frequency bands," *IEEE Access*, vol. 10, pp. 107575–107586, 2022, doi: 10.1109/ACCESS.2022.3212777.